



## N-CQDs accelerating surface charge transfer of $\text{Bi}_4\text{O}_5\text{I}_2$ hollow nanotubes with broad spectrum photocatalytic activity

Mengxia Ji<sup>a</sup>, Yiling Liu<sup>b</sup>, Jun Di<sup>a</sup>, Rong Chen<sup>b</sup>, Zhigang Chen<sup>b</sup>, Jiexiang Xia<sup>a,\*</sup>, Huaming Li<sup>a,\*</sup>

<sup>a</sup> School of Chemistry and Chemical Engineering, Institute for Energy Research, Jiangsu University, 301 Xuefu Road, Zhenjiang, 212013, PR China

<sup>b</sup> School of the Environment and Safety Engineering, Jiangsu University, 301 Xuefu Road, Zhenjiang, 212013, PR China



### ARTICLE INFO

#### Keywords:

N-CQDs  
 $\text{Bi}_4\text{O}_5\text{I}_2$  hollow nanotube  
 Photocatalytic  
 BPA removal  
 Charge separation

### ABSTRACT

Novel N-doped carbon quantum dots (N-CQDs) modified  $\text{Bi}_4\text{O}_5\text{I}_2$  hollow nanotubes photocatalysts have been prepared for the first time.  $\text{Bi}_4\text{O}_5\text{I}_2$  nanomaterials with hollow nanotube structure were designed to shorten the charge carriers' migration distance from bulk phase to surface while the N-CQDs was modified to accelerate the surface charge transfer. Multiple characterization methods have been applied to explore the phase structure, elemental composition, optical absorption properties and photocatalytic performance of as-prepared N-CQDs/ $\text{Bi}_4\text{O}_5\text{I}_2$  composites. The N-CQDs/ $\text{Bi}_4\text{O}_5\text{I}_2$ -0.2 composite showed higher photocatalytic activity for the removal of bisphenol A than pure  $\text{Bi}_4\text{O}_5\text{I}_2$  hollow nanotube under UV light, visible light, light above 580 nm, which exhibited the broad spectrum photocatalytic activity. ESR analysis demonstrated the N-CQDs modification can tune the concentration of reactive oxygen species ( $\cdot\text{OH}$  and  $\cdot\text{O}_2^-$ ). Combined with free radical trapping experiment results, hole,  $\cdot\text{OH}$  and  $\cdot\text{O}_2^-$  were demonstrated to be the main active species and synergistically promoted the enhancement of photocatalytic activity for N-CQDs/ $\text{Bi}_4\text{O}_5\text{I}_2$  composite.

### 1. Introduction

Photocatalysis technology has been regarded as a prospective path in the conversion of solar energy in the field of water splitting [1,2], nitrogen fixation [3,4],  $\text{CO}_2$  reduction [5,6] and environment remediation [7], so as to be able to solve the huge energy demand and worsening environmental issue. Traditional photocatalysts like  $\text{TiO}_2$ ,  $\text{ZnO}$ ,  $\text{CdS}$  are greatly limited by its narrow solar light absorption range, high recombination rate of photogenerated charge carriers, low quantum yield and instability [8–11]. Bi-based semiconductor photocatalysts gradually come into people's sight and have aroused more and more investigate interests for its high visible light photocatalytic performance, structural stability and non-toxic [6,12–18].

Recently,  $\text{BiOX}$  ( $X = \text{Cl}, \text{Br}, \text{I}$ ) as a representative member of Bi-based semiconductor photocatalysts, has drawn lots of attention owing to its unique layered structure, composing of  $[\text{Bi}_2\text{O}_2]$  slabs interleaved with double halogen atoms slabs [3,19–24]. Self-built internal static electric field in the  $\text{BiOX}$  materials could enable excited charge carriers to efficiently separate and transfer from the bulk to surface, thus realize high photogenerated electron-hole separation efficiency. Among these bismuth oxyhalides semiconductor photocatalysts,  $\text{BiOI}$  material exhibits the widest visible light absorption range and satisfying photocatalytic performance under visible light irradiation, arousing extensive

research interests in the field of photocatalysis [20,25–30]. Unfortunately, unsatisfactory charge separation and utilization efficiency in bulk  $\text{BiOI}$  material greatly limits its further application. Series of optimized strategies have been applied to overcome these intrinsic deficiencies, such as morphological controlling, crystal face exposure, heterostructure construction, metal deposition, and so on [31]. The enhanced photocatalytic performance of  $\text{BiOI}$  material could be realized. Recently, Bi-rich strategy has been applied to modulate the light absorption range and valence or conduction band position of the  $\text{BiOX}$  materials to realize a higher photocatalytic activity towards environment remediation [32], hydrogen or oxygen production from water [33],  $\text{CO}_2$  reduction [34] or nitrogen fixation [35], etc. For example, Zhang's group reported the carbon doped  $\text{Bi}_3\text{O}_4\text{Cl}$  exhibits high-performance for photocatalytic  $\text{O}_2$  evolution via giant enhancement of internal electric field [36]. Ye's group found  $\text{Bi}_5\text{O}_7\text{I}$  nanosheets with exposed {001} facets have higher photogenerated charge carriers separation efficiency and increased photocatalytic  $\text{N}_2$  fixation performance than  $\text{Bi}_5\text{O}_7\text{I}$  with {100} facets exposure [37]. The feasible Bi-rich strategy brings us a new sight in improving photocatalytic performance of  $\text{BiOI}$ . A series of Bi-rich bismuth oxyiodide with different morphologies have been synthesized and studied, like 3D hierarchical  $\text{Bi}_4\text{O}_5\text{I}_2$ / $\text{Bi}_5\text{O}_7\text{I}$  microspheres [38],  $\text{Bi}_4\text{O}_5\text{I}_2$  ultrathin nanosheets [31],  $\text{Bi}_5\text{O}_7\text{I}$  nanowires [39] and  $\text{Bi}_7\text{O}_9\text{I}_3$  microspheres [40]. In which,  $\text{Bi}_4\text{O}_5\text{I}_2$

\* Corresponding authors.

E-mail addresses: [xjx@ujs.edu.cn](mailto:xjx@ujs.edu.cn) (J. Xia), [lhm@ujs.edu.cn](mailto:lhm@ujs.edu.cn) (H. Li).

material displays a charming photocatalytic performance for its suitable band gap position and strong response in visible light region [41]. To the best of our knowledge, construction of semiconductor photocatalysts with ultrathin or ultrasmall structures could facilitate the electron-hole pairs' transfer from bulk phase to surface of semiconductors, thus improving the photocatalytic performance. One dimensional structures, including nanowire, nanorod, nanofiber and nanotube, have been widely investigated in various research fields for their great specific surface area, unique facial directed migration for charge carriers and more exposed active sites [42]. In consideration of these, design and synthesis of  $\text{Bi}_4\text{O}_5\text{I}_2$  photocatalyst with hollow nanotube structure is expected to shorten charge carriers migration distance to realize fast charge transfer to the surface of  $\text{Bi}_4\text{O}_5\text{I}_2$  material.

Generally, three crucial steps in a whole photocatalytic reaction, namely light absorption, charge separation and migration, as well as interfacial reactions. Despite the inhibited bulk phase recombination in the  $\text{Bi}_4\text{O}_5\text{I}_2$  photocatalyst could be obtained owing to the hollow nanotube structure, surface-reaching charge would also suffer recombination, which would limit the photocatalytic performance of  $\text{Bi}_4\text{O}_5\text{I}_2$ . Carbon quantum dots (CQDs) with size below 10 nm is regarded as a novel nanocarbon material and has caused wide interests in research for its excellent physicochemical properties, like up-converted photoluminescence behavior, low cost and toxicity, and electron reservoir properties [43,44]. Based on previous research work, it has been demonstrated that the introduction of CQD into photocatalysis field could not only enhance the visible light absorption, but also promote the electron transfer efficiency. Simultaneously, introducing nitrogen into CQDs could efficiently induce charge delocalization, thus facilitating the charge transfer capability of CQDs [45,46]. Inspired by these, it can be designed to construct a bulk-to-surface channel for charge transport from  $\text{Bi}_4\text{O}_5\text{I}_2$  to N-CQDs by introducing N-CQDs into  $\text{Bi}_4\text{O}_5\text{I}_2$  hollow nanotubes, so as to expect a satisfying charge utilization efficiency and photocatalytic performance.

Herein, the novel N-CQDs/ $\text{Bi}_4\text{O}_5\text{I}_2$  nanotubes photocatalysts have been synthesized for the first time. The composition, microstructure, optical and photoelectrical properties of the as-prepared N-CQDs/ $\text{Bi}_4\text{O}_5\text{I}_2$  are studied in detail. The photodegradation experiments over N-CQDs/ $\text{Bi}_4\text{O}_5\text{I}_2$  materials under light irradiation with different wavelength have been carried out towards different pollutants removal to study the key role of N-CQDs. The possible photocatalytic enhancement mechanism has also been proposed based on the XPS valence band spectra, active species trapping experiments and electron spin resonance analysis.

## 2. Experimental section

### 2.1. Preparation of materials

Bismuth nitrate ( $\text{Bi}(\text{NO}_3)_3 \cdot 5\text{H}_2\text{O}$ ), potassium iodide (KI) and ammonium citrate  $\text{C}_6\text{H}_5\text{O}_7(\text{NH}_4)_3$  were analytical pure and used in the experiment as received without any treatment. The N-CQDs solution was prepared according to the literature [20]: 5 mmol  $\text{C}_6\text{H}_5\text{O}_7(\text{NH}_4)_3$  was dissolved in 10 mL  $\text{H}_2\text{O}$  and 335  $\mu\text{L}$  ethylenediamine, then the dispersed solution was poured into a 25 mL autoclave and heated at 200 °C for 5 h. Finally, the sample cooled to the room temperature was dialyzed for 24 h in order to obtain the required N-CQDs solution.

The  $\text{Bi}_4\text{O}_5\text{I}_2$  nanotubes were prepared via a facile solvothermal method with a proper pH value. Typically, 0.5 mmol  $\text{Bi}(\text{NO}_3)_3 \cdot 5\text{H}_2\text{O}$  and 0.2 g PVP was weighed accurately and dissolved into 15 mL mannitol solution (0.1 mol/L) under continuous stirring, then the 5 mL  $\text{H}_2\text{O}$  containing 0.5 mmol KI was added into the above suspension to obtain the mixed solution. The pH value of the mixed solution was adjusted to be 7 by a 1 M NaOH with constantly stirring. The mixed solution was stirred for another 30 min and transferred to a 25 mL autoclave. Immediately, the autoclave was heated at 160 °C for 3 h in a drying oven. The precipitation was collected by a centrifuge and washed using

water and ethanol for several times. The resulting precipitation was the  $\text{Bi}_4\text{O}_5\text{I}_2$  nanotubes.

For the preparation of the N-CQDs/ $\text{Bi}_4\text{O}_5\text{I}_2$  composites, firstly, accurately measuring 0.1, 0.2 and 0.5 mL as-prepared N-CQDs solution into 20 mL  $\text{Bi}_4\text{O}_5\text{I}_2$  nanotubes aqueous solution, respectively, then the N-CQDs/ $\text{Bi}_4\text{O}_5\text{I}_2$  aqueous solution was stirred for 30 min and sonicated for another 30 min. Finally, the obtained product was washed with water and ethanol for several times and dried at 60 °C for one day. The obtained product named as N-CQDs/ $\text{Bi}_4\text{O}_5\text{I}_2$ -0.1, N-CQDs/ $\text{Bi}_4\text{O}_5\text{I}_2$ -0.2, N-CQDs/ $\text{Bi}_4\text{O}_5\text{I}_2$ -0.5, respectively. The certain weight of the added N-CQDs was confirmed using a lyophilizer, and each milliliter N-CQDs solution was weighted to be 47 mg.

### 2.2. Characterization

A Shimadzu XRD-6000 X-ray diffractometer (XRD) was applied to confirm the crystal structure of as-prepared materials with a Cu-K $\alpha$  radiation source. X-ray photoelectron spectroscopy (XPS) spectra of  $\text{Bi}_4\text{O}_5\text{I}_2$  and N-CQDs/ $\text{Bi}_4\text{O}_5\text{I}_2$ -0.2 samples were determined on a VG MultiLab 2000 to analyse the element valence state and chemical composition. A JEOL-JEM-2100 transmission electron microscope (TEM) was used to observe the micro-morphology and structure of as-prepared materials. An UV-2450 Shimadzu UV-vis spectrophotometer was used to confirm the optical adsorption properties of the series of as-prepared photocatalysts, and a blank plate with the pure  $\text{BaSO}_4$  powder as the substrate. A Varian Cary Eclipse spectrometer was employed to investigate the charge carriers' separation of the  $\text{Bi}_4\text{O}_5\text{I}_2$  and N-CQDs/ $\text{Bi}_4\text{O}_5\text{I}_2$ -0.2 samples. A Bruker model ESR JES-FA 200 spectrometer was adopted to determine the active radicals generated over the  $\text{Bi}_4\text{O}_5\text{I}_2$ -based catalysts during the photocatalytic degradation process under visible light irradiation, in which DMPO (Sigma Chemical Co.) in the methanol dispersion for trapping superoxide radicals, DMPO in the aqueous dispersion for trapping hydroxyl radicals. A CHI 660B electrochemical system was employed to analyse the separation and transfer of the photogenerated electron-hole pairs of as-prepared materials. A standard three-electrode system contains a platinum wire as counter electrode, a saturated Ag/AgCl electrode as reference electrode and the  $\text{Bi}_4\text{O}_5\text{I}_2$ -based sample coated ITO glass ( $0.5 \times 1 \text{ cm}^2$ ) as working electrode, respectively. 0.1 M phosphate buffered saline solution adjusting the pH value to be 7 and 0.1 M KCl solution containing 5 mM  $\text{Fe}(\text{CN})_6^{3-}/\text{Fe}(\text{CN})_6^{4-}$  were used for the photocurrent test and electrochemical impedance analysis, respectively.

### 2.3. Photocatalytic activity measurements

A series of photocatalytic degradation experiments under visible light irradiation were performed in a photoreaction chamber with a 300 W Xe lamp and a 400 or 580 nm cutoff filter, while the photocatalytic degradation experiments under ultraviolet (UV) light irradiation were performed in a photoreaction chamber with a 250 W high pressure Hg lamp. During the photocatalytic reaction process, an air pump was taken to realize a constant oxygen supply and a digital circulating water bath was employed to keep the reaction temperature at 30 °C. 30 mg, 30 mg and 20 mg as-prepared photocatalysts was poured into 100 mL target pollutant aqueous solution of bisphenol A (BPA, 10 mg/L), enrofloxacin (ENR, 10 mg/L) and rhodamine B (RhB, 10 mg/L), respectively. Before light up, the mixed solution was stirred for 30 min in the dark to achieve the absorption-desorption equilibrium between pollutant and catalyst. At certain time, 4 mL reaction mixture was sampled and the obtained supernatant liquor by a centrifuge and the concentration of ENR and RhB at different conditions were measured at the maximum absorption peak of 273 and 553 nm, respectively. The concentration of BPA intermediate solution was measured using an Agilent high performance liquid chromatography (HPLC) system equipped with two Varian ProStar210 pumps and a Varian ProStar325 UV-vis detector. The column temperature was 30 °C and the

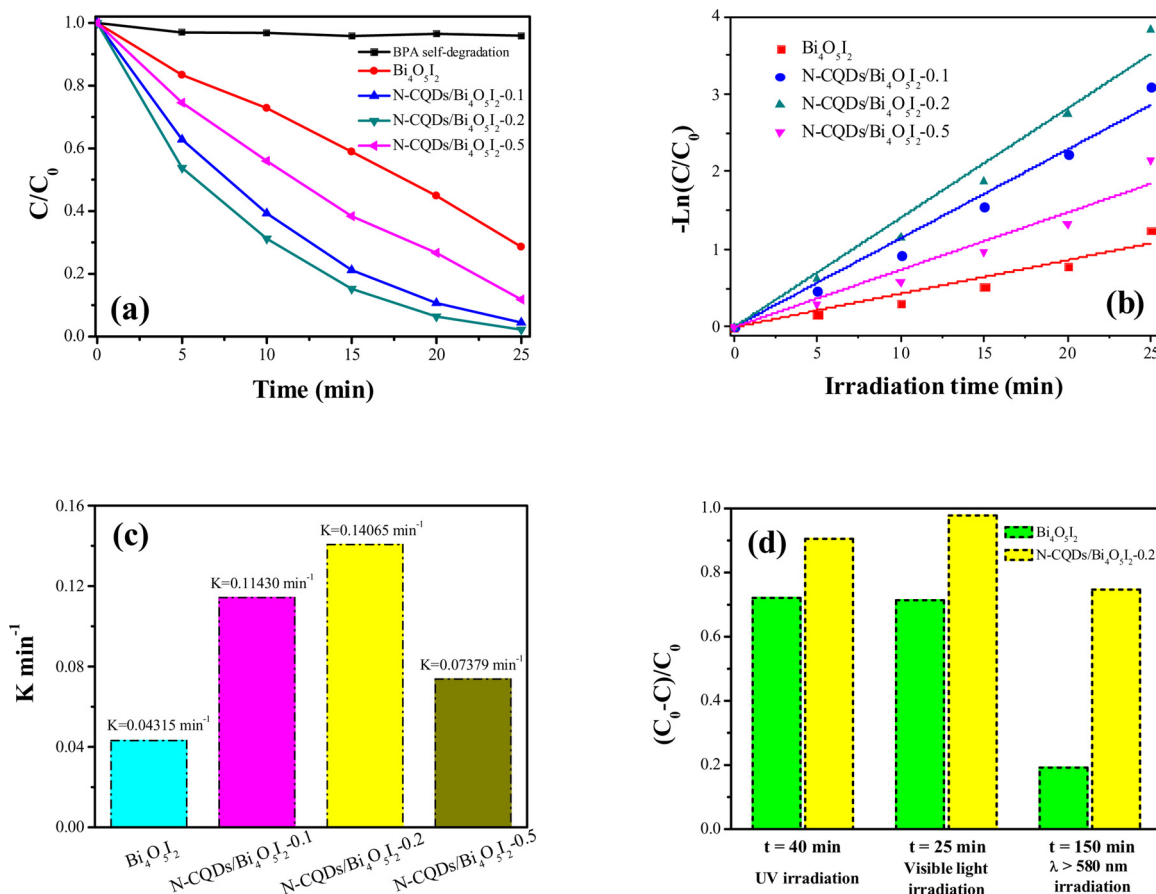


**Fig. 1.** Photocatalytic degradation of BPA (a), corresponding pseudo-first-order kinetic curves (b) and reaction rate constants (c) over as-prepared N-CQDs/ $\text{Bi}_4\text{O}_5\text{I}_2$  and  $\text{Bi}_4\text{O}_5\text{I}_2$  materials under visible light irradiation; comparison of photocatalytic degradation performance of BPA over N-CQDs/ $\text{Bi}_4\text{O}_5\text{I}_2$ -0.2 and  $\text{Bi}_4\text{O}_5\text{I}_2$  materials under light irradiation with different wavelength (d).

detection wavelength was 230 nm. 75% methanol aqueous solution was adopted as the mobile phase and the flow rate was 1.0 mL  $\text{min}^{-1}$ .

### 3. Results and discussion

The photocatalytic performance of the  $\text{Bi}_4\text{O}_5\text{I}_2$  and N-CQDs/ $\text{Bi}_4\text{O}_5\text{I}_2$  composite photocatalysts was evaluated by the photocatalytic degradation of colorless organic pollutant BPA under light irradiation with different wavelengths and the obtained experiment results are in Fig. 1. As shown in Fig. 1a, the BPA self-degradation experiment was carried out to investigate the BPA self-degradation ability during the photocatalytic process under visible light ( $\lambda > 400 \text{ nm}$ ) irradiation. It can be confirmed that the self-degradation ability of BPA can be ignored in the photodegradation experiment. Among as-prepared N-CQDs/ $\text{Bi}_4\text{O}_5\text{I}_2$  and  $\text{Bi}_4\text{O}_5\text{I}_2$  materials, N-CQDs/ $\text{Bi}_4\text{O}_5\text{I}_2$ -0.2 exhibits the highest photocatalytic activity and 93.6% BPA can be removed by N-CQDs/ $\text{Bi}_4\text{O}_5\text{I}_2$ -0.2 after visible light irradiation for 20 min, at the same time, only about 55.1% BPA can be degraded over pure  $\text{Bi}_4\text{O}_5\text{I}_2$  sample. The detailed BPA photodegradation curves have been evaluated by a high performance liquid chromatograph (HPLC) and the corresponding experiment results are shown in Figs. 2a, b and S1. Meanwhile, the intermediates generated during the photocatalytic degradation BPA process were determined using LC-MS analysis. It can be seen that BPA at  $m/z$  227.68 eluted at a retention time (RT) of 5.23 min before visible light irradiation (Fig. 2c) while only one intermediate at  $m/z$  198.39 can be detected at a RT of 3.69 min after visible light irradiated for 5 min (Fig. 2d), and the possible molecular structure of the intermediate has been displayed in the Fig. 2c, d [47]. As shown in Fig. 1b, c, the corresponding pseudo-first-order kinetic curves of photocatalytic

degradation BPA over as-prepared photocatalysts show more clearly that the N-CQDs/ $\text{Bi}_4\text{O}_5\text{I}_2$  composites exhibit the higher rate constants than the pure  $\text{Bi}_4\text{O}_5\text{I}_2$  sample, in which the N-CQDs/ $\text{Bi}_4\text{O}_5\text{I}_2$ -0.2 owns the maximum rate constant ( $K = 0.14065 \text{ min}^{-1}$ ) and is more than three times than the  $\text{Bi}_4\text{O}_5\text{I}_2$  sample ( $K = 0.04315 \text{ min}^{-1}$ ). To further evaluate the photocatalytic activity of the N-CQDs/ $\text{Bi}_4\text{O}_5\text{I}_2$ -0.2 and  $\text{Bi}_4\text{O}_5\text{I}_2$  sample, a series of photoreaction experiments under light irradiation with different wavelength have been carried out. From Fig. 1d, it can be seen that the BPA removal rate over the N-CQDs/ $\text{Bi}_4\text{O}_5\text{I}_2$ -0.2 and  $\text{Bi}_4\text{O}_5\text{I}_2$  sample is about 90.5% and 72.1% after UV light irradiated for 40 min and 97.8% and 71.4% after visible light irradiated for 25 min, respectively. The detailed photodegradation process over N-CQDs/ $\text{Bi}_4\text{O}_5\text{I}_2$ -0.2 and  $\text{Bi}_4\text{O}_5\text{I}_2$  under UV light is shown in Fig. S2. Around 18.4% improvement for N-CQDs/ $\text{Bi}_4\text{O}_5\text{I}_2$ -0.2 composite can be obtained compared with pure  $\text{Bi}_4\text{O}_5\text{I}_2$  under UV light irradiation, which might be profited by the fast interfacial charge carriers' transfer rate via N-CQDs in N-CQDs/ $\text{Bi}_4\text{O}_5\text{I}_2$  composite. It is noteworthy that the N-CQDs/ $\text{Bi}_4\text{O}_5\text{I}_2$  composite exhibits 26.4% higher than  $\text{Bi}_4\text{O}_5\text{I}_2$  with visible light irradiated for 25 min, showing a greater promotion for photodegradation performance than UV irradiation. These results indicate the introduction of N-CQDs into  $\text{Bi}_4\text{O}_5\text{I}_2$  is beneficial for the enhancement of the pure  $\text{Bi}_4\text{O}_5\text{I}_2$  material's photocatalytic activity, especially under visible light irradiation. Based on the previous studies, the introduction of quantum dot could broaden the light absorption range of intrinsic materials, which is beneficial for the improvement of the photocatalytic performance in the visible light region. A 580 nm cut-off filter was used to further investigate the photocatalytic performance for the BPA degradation over N-CQDs/ $\text{Bi}_4\text{O}_5\text{I}_2$ -0.2 and  $\text{Bi}_4\text{O}_5\text{I}_2$  with long-wavelength light irradiation, the result is shown in Fig. 1d

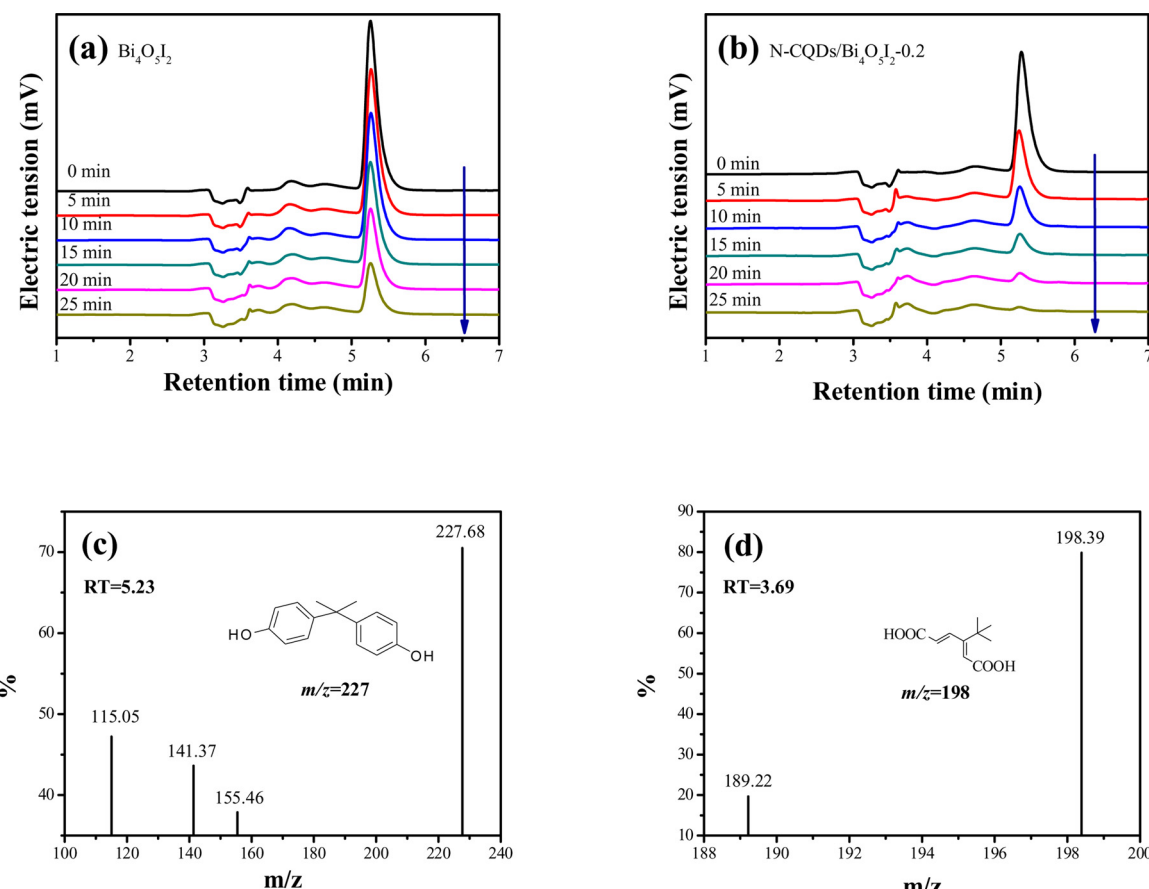


**Fig. 2.** High performance liquid chromatograms (HPLC) of BPA degradation over as-prepared  $\text{Bi}_4\text{O}_5\text{I}_2$  (a) and N-CQDs/ $\text{Bi}_4\text{O}_5\text{I}_2$ -0.2 (b) under visible light irradiation; mass spectra (MS) and corresponding proposed structures at retention times of 5.23 min (c) and 3.69 min (d), respectively.

and the detailed photodegradation process over N-CQDs/ $\text{Bi}_4\text{O}_5\text{I}_2$ -0.2 and  $\text{Bi}_4\text{O}_5\text{I}_2$  under  $\lambda > 580$  nm light are shown in Fig. S3. It can be seen obviously that only 19.2% BPA can be degraded by pure  $\text{Bi}_4\text{O}_5\text{I}_2$  material while 74.7% BPA can be degraded by the N-CQDs/ $\text{Bi}_4\text{O}_5\text{I}_2$ -0.2 composite after visible light ( $\lambda > 580$  nm) irradiated for 150 min, which BPA removal rate is about 3.3 times higher than the pure  $\text{Bi}_4\text{O}_5\text{I}_2$  material. The degradation curves under light irradiation at different wavelength region strongly indicate that N-CQDs in the  $\text{Bi}_4\text{O}_5\text{I}_2$  material played a crucial role in enhancing the photocatalytic performance under UV or long-wavelength light irradiation. The N-CQDs/ $\text{Bi}_4\text{O}_5\text{I}_2$  nanocomposites with broad spectrum photocatalytic activity for pollutant removal have been synthesized successfully. Concurrently, photocatalytic degradation experiments of ENR and RhB were evaluated and the corresponding results are shown in Fig. S4. Meanwhile, pseudo-first-order rate constants of photocatalytic degradation BPA, ENR and RhB over N-CQDs/ $\text{Bi}_4\text{O}_5\text{I}_2$ -0.2 and  $\text{Bi}_4\text{O}_5\text{I}_2$  materials under visible light irradiation have been listed in Table S1, it can be intuitively seen that the introduction of N-CQDs is beneficial for the  $\text{Bi}_4\text{O}_5\text{I}_2$  material to obtain the superior photocatalytic activity and N-CQDs/ $\text{Bi}_4\text{O}_5\text{I}_2$ -0.2 composite exhibits the highest photocatalytic activity for organic pollutant removal.

To ascertain whether the crystal structures and crystalline phases of  $\text{Bi}_4\text{O}_5\text{I}_2$  samples changed after adding N-CQDs stock solution, X-ray diffraction (XRD) patterns of as-prepared  $\text{Bi}_4\text{O}_5\text{I}_2$  and N-CQDs/ $\text{Bi}_4\text{O}_5\text{I}_2$  materials with different N-CQDs content have been obtained and are shown in Fig. 3. All of the diffraction peaks of as-prepared materials located at  $28.8^\circ$ ,  $31.5^\circ$ ,  $36.9^\circ$ ,  $42.1^\circ$ ,  $45.1^\circ$ ,  $49.3^\circ$  and  $54.4^\circ$  in XRD pattern can be indexed to  $(-4 -1 1)$ ,  $(4 0 2)$ ,  $(-4 0 4)$ ,  $(-3 2 3)$ ,  $(4 2 2)$ ,  $(0 0 6)$  and  $(8 1 1)$  planes of  $\text{Bi}_4\text{O}_5\text{I}_2$ , which are according to the previous literature [31,34,47–49]. No typical peaks of N-CQDs can be

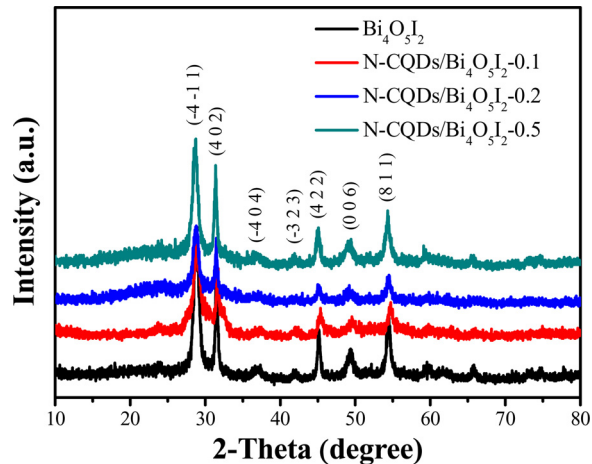


**Fig. 3.** XRD patterns of as-prepared  $\text{Bi}_4\text{O}_5\text{I}_2$  and N-CQDs/ $\text{Bi}_4\text{O}_5\text{I}_2$  composites.

found in the XRD pattern of N-CQDs/ $\text{Bi}_4\text{O}_5\text{I}_2$  materials, which could be ascribed to the low amount of N-CQDs in the N-CQDs/ $\text{Bi}_4\text{O}_5\text{I}_2$  materials. In addition, no other peaks have been observed in the picture, indicating the  $\text{Bi}_4\text{O}_5\text{I}_2$  and N-CQDs/ $\text{Bi}_4\text{O}_5\text{I}_2$  materials with high purity have been successfully synthesized.

XPS analysis is employed to determine the chemical state and elemental composition of as-prepared N-CQDs/ $\text{Bi}_4\text{O}_5\text{I}_2$ -0.2 composite and  $\text{Bi}_4\text{O}_5\text{I}_2$  material, the XPS survey spectra and high-solution spectra are shown in Fig. 4. It can be seen that five different elements C, N, Bi, O and I in N-CQDs/ $\text{Bi}_4\text{O}_5\text{I}_2$ -0.2 composite in Fig. 4a. The binding energies of 158.0 and 163.4 eV for pure  $\text{Bi}_4\text{O}_5\text{I}_2$  material are belonged to Bi 4f7/

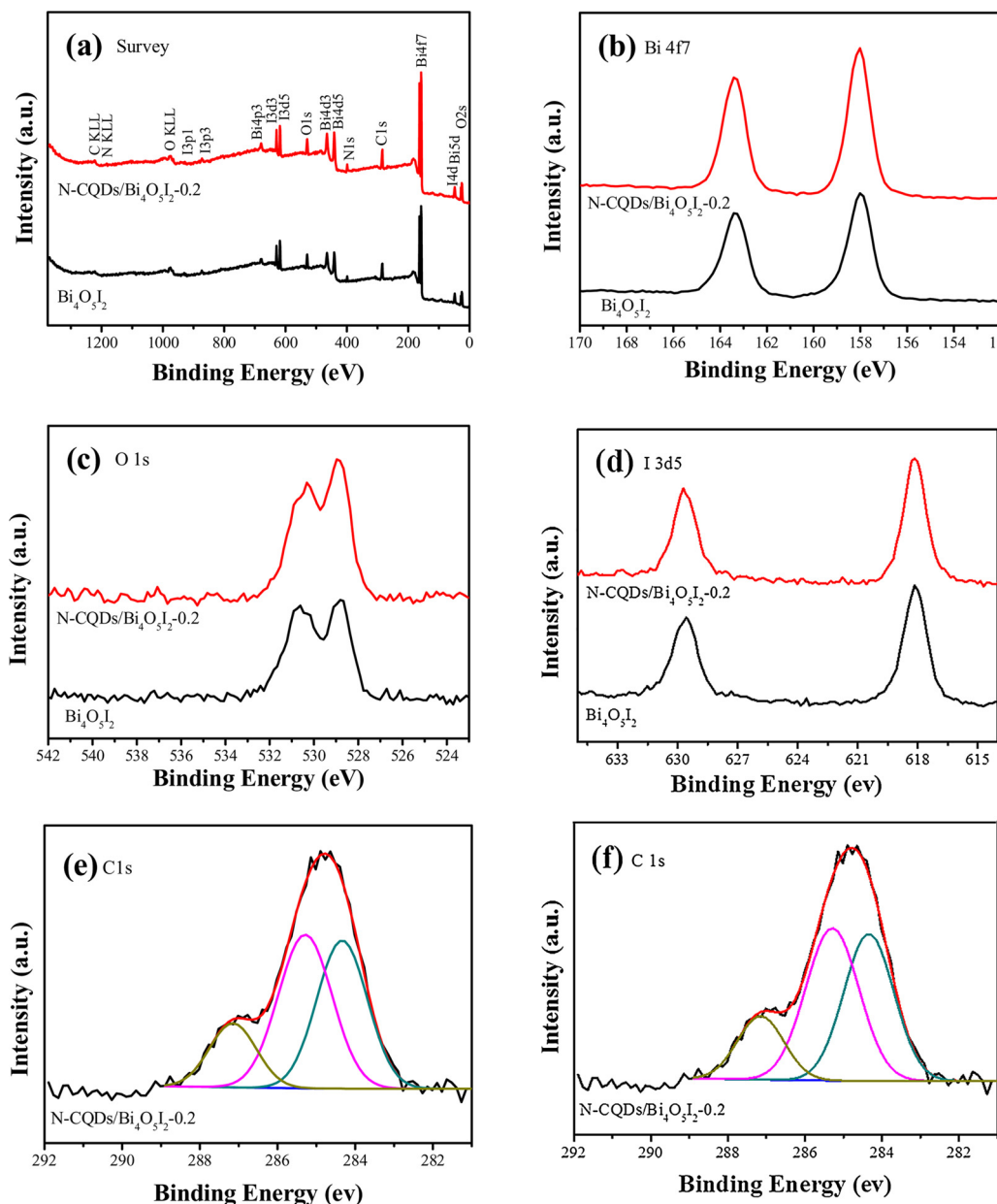


**Fig. 4.** XPS spectra: full scan (a), Bi 4f (b), O 1s (c) and I 3d (d) of Bi<sub>4</sub>O<sub>5</sub>I<sub>2</sub> and CQDs/Bi<sub>4</sub>O<sub>5</sub>I<sub>2</sub>-0.2 samples; C 1s (e) and N 1s (f) of N-CQDs/Bi<sub>4</sub>O<sub>5</sub>I<sub>2</sub>-0.2 sample.

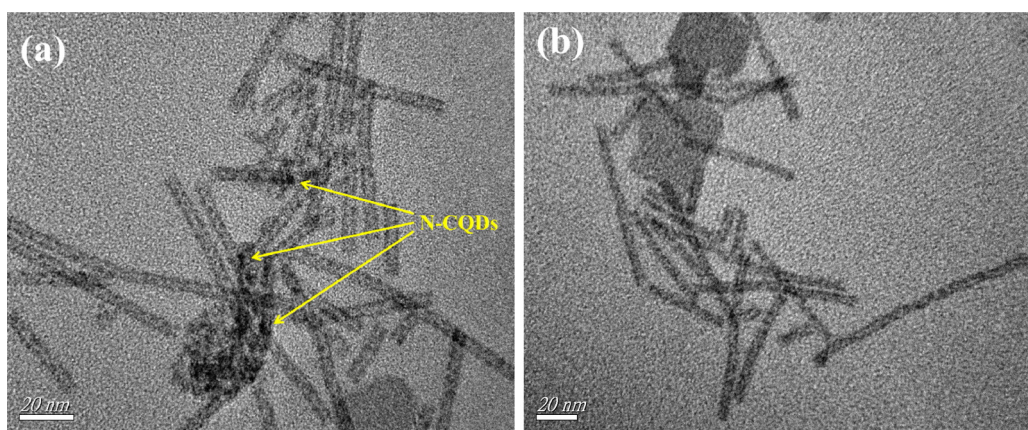


**Fig. 5.** TEM images of N-CQDs/Bi<sub>4</sub>O<sub>5</sub>I<sub>2</sub>-0.2 composite.

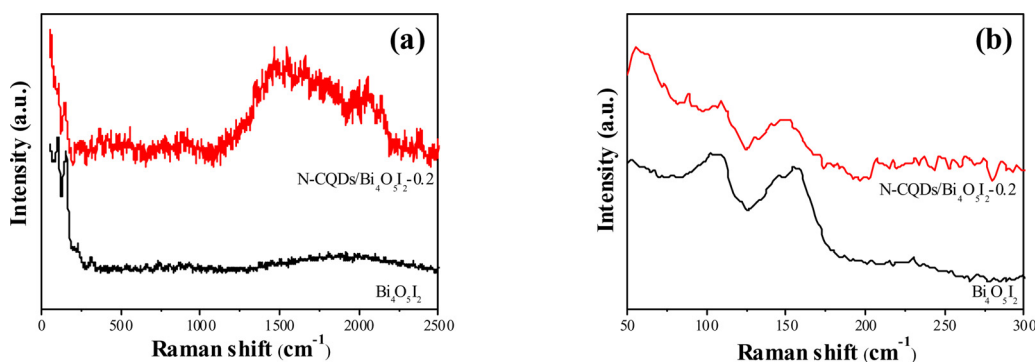


Fig. 6. Raman shift (a) and partial enlarged Raman spectra detail (b) of Bi<sub>4</sub>O<sub>5</sub>I<sub>2</sub> and N-CQDs/Bi<sub>4</sub>O<sub>5</sub>I<sub>2</sub>-0.2 composite.

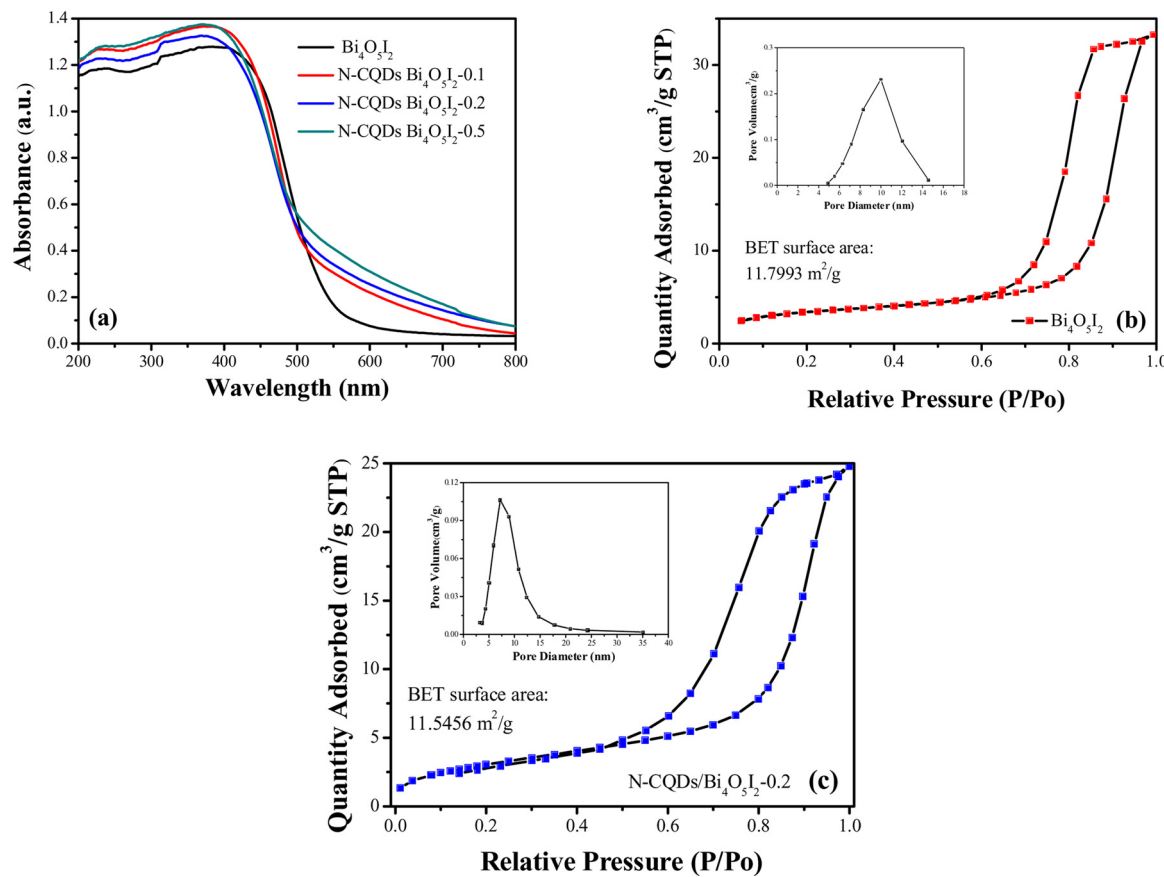
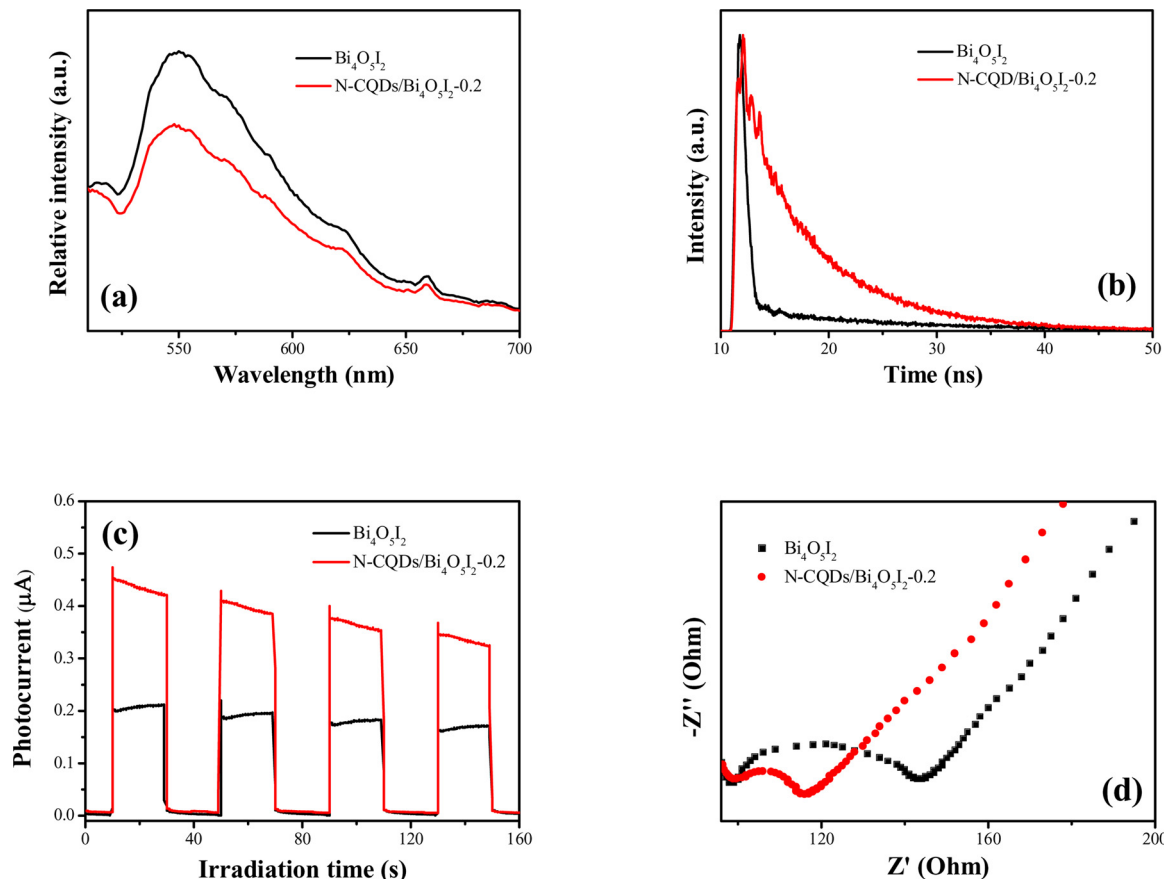


Fig. 7. UV-vis optical absorption spectroscopy of series of N-CQDs/Bi<sub>4</sub>O<sub>5</sub>I<sub>2</sub> composites and pure Bi<sub>4</sub>O<sub>5</sub>I<sub>2</sub> (a); nitrogen adsorption-desorption isotherm and the corresponding pore-size distribution of N-CQDs/Bi<sub>4</sub>O<sub>5</sub>I<sub>2</sub>-0.2 (b).

2 and Bi 4f5/2, respectively. No obvious shift of the characteristic peaks in N-CQDs/Bi<sub>4</sub>O<sub>5</sub>I<sub>2</sub>-0.2 composite can be observed (Fig. 4b), which could be speculated that the surface-modified N-CQDs did not change the surface Bi chemical environment of pure Bi<sub>4</sub>O<sub>5</sub>I<sub>2</sub>. Fig. 4c exhibits the high-resolution O 1s spectra of the N-CQDs/Bi<sub>4</sub>O<sub>5</sub>I<sub>2</sub>-0.2 composite, the peak at 530.3 eV is assigned to the O<sup>2-</sup> in the Bi<sub>4</sub>O<sub>5</sub>I<sub>2</sub> material. Two peaks at 618.2 and 629.6 eV as shown in Fig. 4d are attributed to I 3d5/2 and I 3d3/2, respectively, which is corresponding to the iodine in the Bi<sub>4</sub>O<sub>5</sub>I<sub>2</sub>. There is also no obvious shift could be observed in the I 3d high-resolution of the two materials, it further confirms the introduction of N-CQDs using facile ultrasonic method did not change the surface chemical environment of Bi<sub>4</sub>O<sub>5</sub>I<sub>2</sub> material. In the high-resolution C 1s spectra (Fig. 4e), three peaks at 284.4, 285.3 and 287.2 eV are belonged to the C=C/C=C, oxygenated carbon, and nitrous carbon, respectively [43]. As shown in Fig. 4f, the N 1s peak located at 399.2 eV is

assigned to N–H in the N-CQDs. The XPS analysis results demonstrate the successful introduction of N-CQDs into Bi<sub>4</sub>O<sub>5</sub>I<sub>2</sub> material and the N-CQDs/Bi<sub>4</sub>O<sub>5</sub>I<sub>2</sub> composite material has been synthesized. FT-IR spectrum has been employed to further determine the coexistence of N-CQDs and Bi<sub>4</sub>O<sub>5</sub>I<sub>2</sub> in the N-CQDs/Bi<sub>4</sub>O<sub>5</sub>I<sub>2</sub> composite. It can be seen in Fig. S5, the characteristic peaks of as-prepared photocatalysts at 545.1 cm<sup>-1</sup> are belonged to the Bi-O stretching mode. The peaks at 1544.0 cm<sup>-1</sup> of N-CQDs modified Bi<sub>4</sub>O<sub>5</sub>I<sub>2</sub> composites gradually strengthen with the increasing content of the N-CQDs in the system, which can be assigned to the bending vibrations of N-H. The FT-IR and XPS results indicate the N-CQDs have been successfully introduced to the Bi<sub>4</sub>O<sub>5</sub>I<sub>2</sub> material.

Fig. 5 shows the TEM images of N-CQDs/Bi<sub>4</sub>O<sub>5</sub>I<sub>2</sub>-0.2 composite to observe the morphology and microstructure. It can be seen that as-prepared Bi<sub>4</sub>O<sub>5</sub>I<sub>2</sub> material is composed of lots of hollow nanotubes, and the diameter of these hollow nanotubes is less than 5 nm. The hollow



**Fig. 8.** Steady-state PL spectra (a), time-resolved transient PL decay spectra (b), transient photocurrent response (c) and electrochemical impedance spectroscopy (d) of pure  $\text{Bi}_4\text{O}_5\text{I}_2$  and N-CQDs/ $\text{Bi}_4\text{O}_5\text{I}_2$ -0.2 composite.

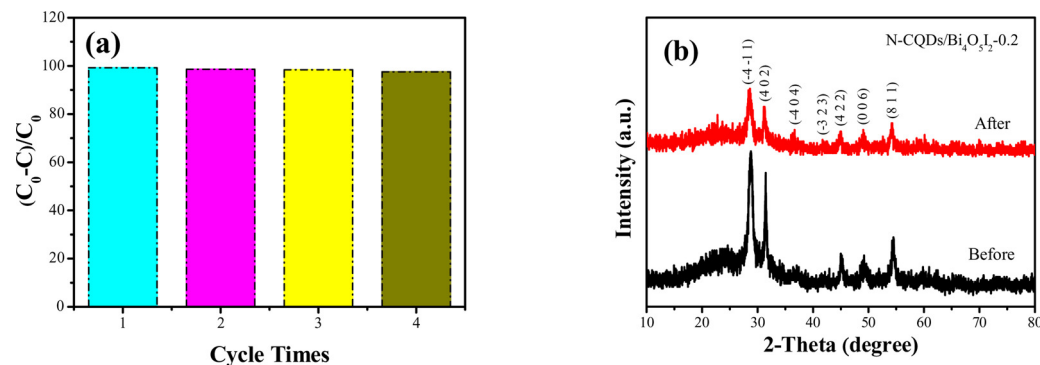


**Fig. 9.** Cycle experiments for photocatalytic degradation BPA under visible light irradiation (a) and XRD patterns before and after four cycles (b) over N-CQDs/ $\text{Bi}_4\text{O}_5\text{I}_2$ -0.2 composite.

structure can provide more exposed surface area to adsorb the N-CQDs and more active sites for pollutant degradation. Some dark dots with 2–3 nm diameters attached on the surface of  $\text{Bi}_4\text{O}_5\text{I}_2$  nanotubes (Fig. 5a) demonstrate N-CQDs have been successfully introduced into  $\text{Bi}_4\text{O}_5\text{I}_2$ . To further confirm the existence of N-CQDs, the elemental mapping measurement was performed and the corresponding analysis results are displayed in Fig. S6. From the pictures it can be demonstrated that there are five main elements Bi, O, I, C and N in the N-CQDs/ $\text{Bi}_4\text{O}_5\text{I}_2$ -0.2 composite, respectively, and the elements C and N are distributed on the surface of  $\text{Bi}_4\text{O}_5\text{I}_2$  hollow nanotubes uniformly. The obtained results are consistent with FT-IR and XPS analysis results.

Raman technique has been employed to investigate the structural changes of the pure  $\text{Bi}_4\text{O}_5\text{I}_2$  and N-CQDs/ $\text{Bi}_4\text{O}_5\text{I}_2$ -0.2 composite and the corresponding results are shown in Fig. 6. The vibrational peaks around

at 108 and 153  $\text{cm}^{-1}$  in Fig. 6a (the corresponding enlarged view from 50 to 300  $\text{cm}^{-1}$  is shown in Fig. 6b) could be attributed to the  $\text{A}_{1g}$  and  $\text{E}_g$  Bi-I internal stretching mode of  $\text{Bi}_4\text{O}_5\text{I}_2$ , respectively [50,51]. Two obvious Raman peaks of a D band and G band located at 1357 and 1545  $\text{cm}^{-1}$  of the N-CQDs/ $\text{Bi}_4\text{O}_5\text{I}_2$ -0.2 composite can be observed clearly indicating the existence of carbon atoms [52], which further confirm the N-CQDs have been successfully compounded with the  $\text{Bi}_4\text{O}_5\text{I}_2$  hollow nanotubes. However, strong background interference appeared in N-CQDs/ $\text{Bi}_4\text{O}_5\text{I}_2$ -0.2 is attributed to the strong fluorescence of N-CQDs [53].

UV-vis diffuse reflectance spectra (DRS) have been recorded to explore the light-absorption ability of the N-CQDs/ $\text{Bi}_4\text{O}_5\text{I}_2$  composites and  $\text{Bi}_4\text{O}_5\text{I}_2$  hollow nanotubes. The light-absorption edge of the pure  $\text{Bi}_4\text{O}_5\text{I}_2$  hollow nanotubes can be determined to be 560 nm from Fig. 7a.

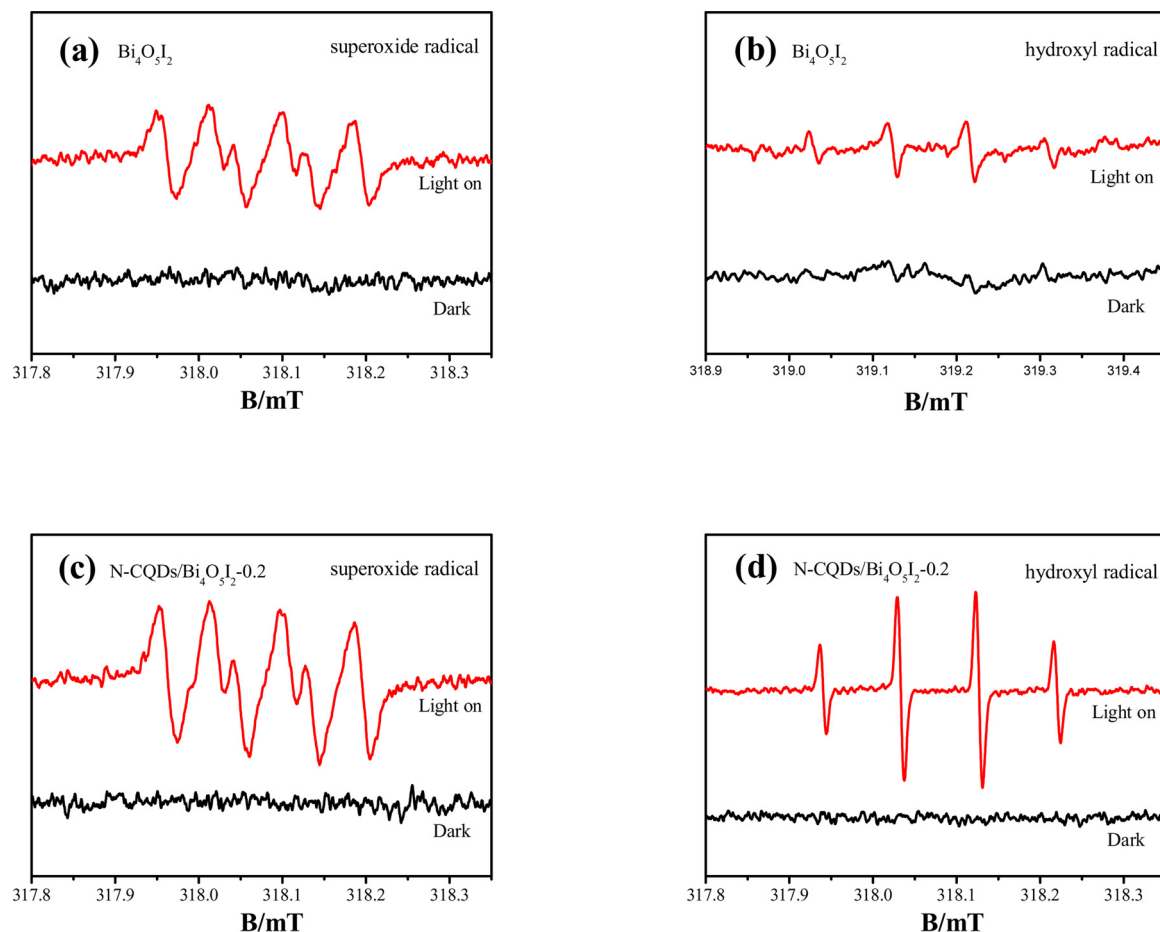


**Fig. 10.** DMPO spin-trapping ESR spectra of  $\text{Bi}_4\text{O}_5\text{I}_2$  (a, b) and N-CQDs/ $\text{Bi}_4\text{O}_5\text{I}_2$ -0.2 (c, d) without or with visible light irradiation.

No significant change of the light-absorption edge for the as-prepared N-CQDs/ $\text{Bi}_4\text{O}_5\text{I}_2$  composites can be seen in DRS, however, an enhanced additional exponentially decaying absorption tails among the whole visible light region can be observed with the increasing content of N-CQDs. This phenomenon further confirms the co-existence of the  $\text{Bi}_4\text{O}_5\text{I}_2$  hollow nanotubes and N-CQDs. The enhanced visible-light absorption ability of as-synthesized composites is beneficial for the improvement of the photocatalytic activity, which is consistent with the BPA photodegradation experiment results under light irradiation with different wavelength. The reduced photodegradation ability of the N-CQDs/ $\text{Bi}_4\text{O}_5\text{I}_2$ -0.5 composite may be ascribed to the excessive N-CQDs adsorbed on the surface of  $\text{Bi}_4\text{O}_5\text{I}_2$  hollow nanotubes greatly hinder the light absorption of pure  $\text{Bi}_4\text{O}_5\text{I}_2$  material.

To better understand the specific surface areas and pore size distribution of  $\text{Bi}_4\text{O}_5\text{I}_2$  materials after introducing N-CQDs, nitrogen adsorption-desorption isotherms of as-prepared  $\text{Bi}_4\text{O}_5\text{I}_2$ -based materials have been performed. As can be seen in Fig. 7b, c, the BET specific surface areas of  $\text{Bi}_4\text{O}_5\text{I}_2$  ( $11.7993 \text{ m}^2 \text{ g}^{-1}$ ) and N-CQDs/ $\text{Bi}_4\text{O}_5\text{I}_2$ -0.2 ( $11.5456 \text{ m}^2 \text{ g}^{-1}$ ) exhibit no obvious difference, indicating a small quantity of N-CQDs modified on the  $\text{Bi}_4\text{O}_5\text{I}_2$  nanotubes has no impact on the surface of  $\text{Bi}_4\text{O}_5\text{I}_2$ . It could be initially judged that the BET specific surface area is not the main factor affecting the photoreaction performance of N-CQDs/ $\text{Bi}_4\text{O}_5\text{I}_2$  composites.

To investigate the separation and transport efficiency of the photogenerated charge carriers in this system, a series of measurements have been applied. All of the test results are demonstrated in Fig. 8. The steady-state PL spectra and time-resolved transient PL decay spectra of pure  $\text{Bi}_4\text{O}_5\text{I}_2$  and N-CQDs/ $\text{Bi}_4\text{O}_5\text{I}_2$ -0.2 are shown in Fig. 8a, b to study the lifetime of photogenerated charge carriers in the samples. The prolonged lifetime of charge carriers during a degradation reaction

under light irradiation is regarded as a crucial factor in enhancing the photocatalytic activity. In Fig. 8a, the emission peak intensity centered at 550 nm of N-CQDs/ $\text{Bi}_4\text{O}_5\text{I}_2$ -0.2 composite is lower than the pure  $\text{Bi}_4\text{O}_5\text{I}_2$ , indicating the less charge carriers in the N-CQDs/ $\text{Bi}_4\text{O}_5\text{I}_2$ -0.2 would recombine during the photocatalytic process. The time-resolved transient PL decay curves of  $\text{Bi}_4\text{O}_5\text{I}_2$  and N-CQDs/ $\text{Bi}_4\text{O}_5\text{I}_2$ -0.2 are shown in Fig. 8b. The prolonged radiative lifetime fully confirms the introduction of N-CQDs can inhibit the high recombination rate of charge carriers in pure  $\text{Bi}_4\text{O}_5\text{I}_2$  material. The electrochemical methods have also been carried out to better understand the separation and migration efficiency of photoinduced electron-hole pairs in the N-CQDs/ $\text{Bi}_4\text{O}_5\text{I}_2$ -0.2 and  $\text{Bi}_4\text{O}_5\text{I}_2$ . Higher photocurrent response indicates more electrons can be generated to participate in a degradation reaction under light irradiation, thus favor the enhancement of photocatalytic performance. In Fig. 8c, it can be seen that N-CQDs modified  $\text{Bi}_4\text{O}_5\text{I}_2$  nanotube owns the higher photocurrent response than pure  $\text{Bi}_4\text{O}_5\text{I}_2$  material, which could be attributed to the introduction of N-CQDs with high electron conducting capability. The EIS analysis in Fig. 8d shows the smaller diameter of Nyquist circle of N-CQDs/ $\text{Bi}_4\text{O}_5\text{I}_2$ -0.2 composite, supposing the smaller resistance for interfacial charge carriers' transfer process in the N-CQDs/ $\text{Bi}_4\text{O}_5\text{I}_2$ -0.2 composite. Overall consideration of these PL and electrochemical characterization results, it could be confirmed the photogenerated electron-hole pairs can be well separated and transferred from the bulk to the interface of the  $\text{Bi}_4\text{O}_5\text{I}_2$  nanotubes after introducing N-CQDs, which can promote the enhancement of photodegradation performance of  $\text{Bi}_4\text{O}_5\text{I}_2$  nanotubes under light irradiation. These analysis results are in consistent with the photocatalytic degradation experiment results.

Impressive cycle performance and well structural stability are the vital factors to measure a photocatalyst for its further practical

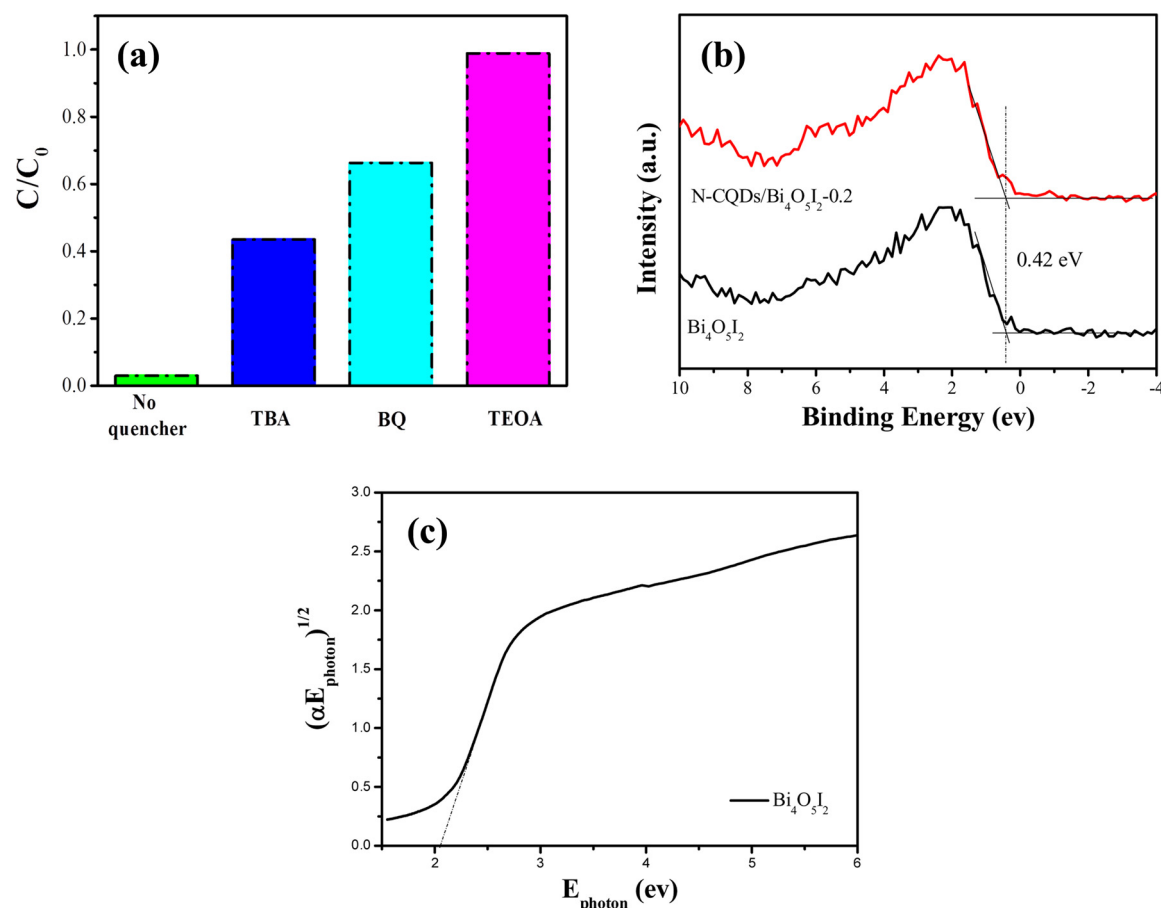


**Fig. 11.** Free radicals trapping experiments of N-CQDs/Bi<sub>4</sub>O<sub>5</sub>I<sub>2</sub>-0.2 composite with the addition of different trapping agents: TBA for •OH, BQ for •O<sub>2</sub><sup>−</sup>, and TEOA for hole, respectively (a), XPS Valence-band spectra of Bi<sub>4</sub>O<sub>5</sub>I<sub>2</sub> and N-CQDs/Bi<sub>4</sub>O<sub>5</sub>I<sub>2</sub>-0.2 (b) and bandgap of pure Bi<sub>4</sub>O<sub>5</sub>I<sub>2</sub> via the classical Tauc plot (c).

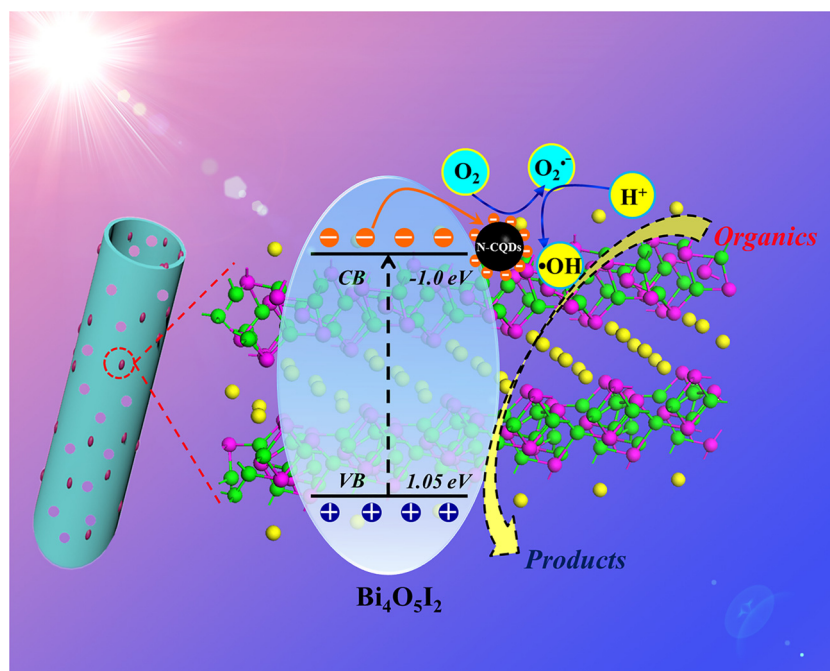


**Fig. 12.** Schematic diagram illuminating the possible separation and transfer of photogenerated electron-hole pairs from bulk Bi<sub>4</sub>O<sub>5</sub>I<sub>2</sub> to N-CQDs under light irradiation.

application. Thus, to investigate thoroughly the structural stability and reliable performance of as-prepared N-CQDs/Bi<sub>4</sub>O<sub>5</sub>I<sub>2</sub>-0.2 composite photocatalyst, cycle experiments of photocatalytic degradation BPA under visible light irradiation have been carried out. There is almost no decrease of the photocatalytic performance could be observed after four cycles in Fig. 9a, demonstrating the N-CQDs/Bi<sub>4</sub>O<sub>5</sub>I<sub>2</sub> composite owns a higher degree of stability in pollutant removal. No other impurity peaks and obvious shift in the XRD pattern (Fig. 9b) and Raman spectra (Fig. S7) for N-CQDs/Bi<sub>4</sub>O<sub>5</sub>I<sub>2</sub>-0.2 composite after the cycle can be discovered, meanwhile, five main elements in N-CQDs/Bi<sub>4</sub>O<sub>5</sub>I<sub>2</sub> can also be found with elemental mapping measurement (Fig. S8), which further confirming the structure of N-CQDs/Bi<sub>4</sub>O<sub>5</sub>I<sub>2</sub> composite is still in high stability and integrality after cycle experiment. Therefore, as-prepared N-CQDs/Bi<sub>4</sub>O<sub>5</sub>I<sub>2</sub> composite with superior photocatalytic performance for organic pollutant removal and high stability is expected for further application.

In a typical photocatalytic degradation process towards organic pollutants, holes generated under light irradiation ( $h\nu \geq E_g$ ) or reactive oxygen species, such as hydroxyl radicals (•OH) and superoxide radicals (•O<sub>2</sub><sup>−</sup>), derived from the activation of surface adsorbed water or hydroxyl groups by holes and electrons can directly participate in the redox reaction for their fascinating oxidizing or reducing ability. Therefore, the efficient utilization of the photogenerated electrons and holes plays a decisive role in a photocatalytic reaction. ESR technique is usually adopted to determine the active species •OH and •O<sub>2</sub><sup>−</sup> products generated under light irradiation, with 5,5-dimethyl-1-pyrroline N-oxide (DMPO) in H<sub>2</sub>O and methanol, respectively [54–57]. Fig. 10 shows the results of ESR analysis for Bi<sub>4</sub>O<sub>5</sub>I<sub>2</sub> and N-CQDs/Bi<sub>4</sub>O<sub>5</sub>I<sub>2</sub>-0.2 composite material with or without visible light irradiation, it can be seen that both •OH and •O<sub>2</sub><sup>−</sup> species can be produced in pure Bi<sub>4</sub>O<sub>5</sub>I<sub>2</sub> and N-CQDs/Bi<sub>4</sub>O<sub>5</sub>I<sub>2</sub>-0.2 composite. After the introduction of N-CQDs in Bi<sub>4</sub>O<sub>5</sub>I<sub>2</sub> nanotubes, the significantly enhanced ESR characteristic signal of •OH and •O<sub>2</sub><sup>−</sup> species in N-CQDs/Bi<sub>4</sub>O<sub>5</sub>I<sub>2</sub>-0.2 composite can be observed in Fig. 10c, d. From ESR analysis, it could be preliminarily concluded that •OH and •O<sub>2</sub><sup>−</sup> are the main active species for the degradation of organic pollutants over N-CQDs/Bi<sub>4</sub>O<sub>5</sub>I<sub>2</sub>-0.2 under visible light irradiation. The obtained results indicate that with the introduction of N-CQDs, the improved separation efficiency of photogenerated electron-hole pairs could be realized in N-CQDs modified Bi<sub>4</sub>O<sub>5</sub>I<sub>2</sub> nanotubes, thus caused higher concentration of reactive oxygen species (•OH and •O<sub>2</sub><sup>−</sup>) in N-CQDs/Bi<sub>4</sub>O<sub>5</sub>I<sub>2</sub>-0.2 composites. Free radicals trapping experiments were also performed to further confirm the main active species in the photodegradation process. It can be seen in Fig. 11a, approximately 97% RhB can be removed over N-CQDs/Bi<sub>4</sub>O<sub>5</sub>I<sub>2</sub>-0.2 under visible light irradiation without adding trapping agent, however, only 56% and 1% RhB can be degraded over N-CQDs/Bi<sub>4</sub>O<sub>5</sub>I<sub>2</sub>-0.2 after adding tertiary butanol (TBA) and triethanolamine (TEOA), respectively, which were chosen as the trapping agents for •OH and hole species. Meanwhile, benzoquinone (BQ) and N<sub>2</sub> were used as the trapping agents for •O<sub>2</sub><sup>−</sup>, a greatly inhibition could be found in the degradation of RhB. These results indicate the hole, •O<sub>2</sub><sup>−</sup> and •OH play vital roles in the photodegradation pollutant process [56,58]. Combined with ESR results, hole, •OH and •O<sub>2</sub><sup>−</sup> active species are demonstrated to participate in the photocatalytic degradation reactions together and synergistically facilitate the enhancement of photocatalytic activity for N-CQDs/Bi<sub>4</sub>O<sub>5</sub>I<sub>2</sub>-0.2.

The valence band (VB) positions of as-prepared Bi<sub>4</sub>O<sub>5</sub>I<sub>2</sub> and N-CQDs/Bi<sub>4</sub>O<sub>5</sub>I<sub>2</sub>-0.2 composite have been ascertained by the XPS valence spectra and the results are exhibited in Fig. 11b. The highest occupied electronic density of state for Bi<sub>4</sub>O<sub>5</sub>I<sub>2</sub> is determined to be 0.42 eV and N-CQDs/Bi<sub>4</sub>O<sub>5</sub>I<sub>2</sub>-0.2 owns the similar valence-band maximum value, which indicates N-CQDs surface modification has no influence on the electronic structure. The results are in accordance with the XPS analysis. A corrected value about 0.63 eV (reference to normal hydrogen electrode (NHE) at pH 7) is introduced for the XPS valence spectra and the VBM for Bi<sub>4</sub>O<sub>5</sub>I<sub>2</sub> is calculated to be 1.05 eV [59]. The band gap ( $E_g$ )

of Bi<sub>4</sub>O<sub>5</sub>I<sub>2</sub> is determined to be 2.05 eV using the classical Tauc plot, the obtained curve is shown in Fig. 11c. According to the energy band calculation formula  $E_{CB} = E_V - E_g$ , the conduction-band minimum (CBM) of Bi<sub>4</sub>O<sub>5</sub>I<sub>2</sub> could be determined to be −1.0 eV. For the consideration of redox potentials for O<sub>2</sub>/•O<sub>2</sub><sup>−</sup> (−0.046 eV vs. NHE) and •OH/OH<sup>−</sup> (+2.38 eV vs. NHE) [20], •O<sub>2</sub><sup>−</sup> can be produced via Bi<sub>4</sub>O<sub>5</sub>I<sub>2</sub> nanotubes while no •OH could be generated during photocatalytic process under visible light irradiation. From ESR analysis, apparent sextet signals of DMPO-•O<sub>2</sub><sup>−</sup> in Bi<sub>4</sub>O<sub>5</sub>I<sub>2</sub> and N-CQDs/Bi<sub>4</sub>O<sub>5</sub>I<sub>2</sub>-0.2 under visible light irradiation prove the •O<sub>2</sub><sup>−</sup> can be generated over Bi<sub>4</sub>O<sub>5</sub>I<sub>2</sub> and N-CQDs/Bi<sub>4</sub>O<sub>5</sub>I<sub>2</sub>-0.2 materials, respectively. Compared with Bi<sub>4</sub>O<sub>5</sub>I<sub>2</sub>, obviously increased DMPO-•O<sub>2</sub><sup>−</sup> signals of N-CQDs/Bi<sub>4</sub>O<sub>5</sub>I<sub>2</sub>-0.2 indicate that the N-CQDs on the Bi<sub>4</sub>O<sub>5</sub>I<sub>2</sub> nanotubes as the charge separation centers promote the effective separation for the photo-induced electron-hole pairs, thus more electrons can be utilized to activate molecular oxygen to produce •O<sub>2</sub><sup>−</sup>. However, different from the calculation result based on redox potential of •OH, ESR and free radicals trapping experiments show the discernible DMPO-•OH signals and significant inhibitory effect of photodegradation RhB activity, demonstrating the generation of •OH. Hence, a possible reaction route to generate •OH by •O<sub>2</sub><sup>−</sup> (2•O<sub>2</sub><sup>−</sup> + 2H<sup>+</sup> → 2•OH + O<sub>2</sub>) will be pointed out. Due to more •O<sub>2</sub><sup>−</sup> reactive species could be generated by N-CQDs/Bi<sub>4</sub>O<sub>5</sub>I<sub>2</sub>-0.2 composites under visible light irradiation for the fast electron transfer by N-CQDs, some excess •O<sub>2</sub><sup>−</sup> could react with H<sup>+</sup> to yield •OH. A possible photocatalytic degradation mechanism has been proposed in Fig. 12. When the visible light irradiation, the electrons will be excited and transfer from VB to CB of Bi<sub>4</sub>O<sub>5</sub>I<sub>2</sub> nanotubes. After the N-CQDs modified on the surface of Bi<sub>4</sub>O<sub>5</sub>I<sub>2</sub> nanotubes, more and more excited electrons could be transferred to the surface of N-CQDs and participate in the following series of redox reactions. Benefiting from the efficient utilization of charge carriers, more of the surface adsorbed oxygen could be reduced to produce abundant •O<sub>2</sub><sup>−</sup> and the excess •O<sub>2</sub><sup>−</sup> would further take part in the reaction to produce •OH. Therefore, the main reactive species including hole, •O<sub>2</sub><sup>−</sup> and •OH generated under light irradiation engage in the organic pollutant removal together, synergistically facilitating the improvement of photocatalytic performance of the N-CQDs/Bi<sub>4</sub>O<sub>5</sub>I<sub>2</sub> composites.

#### 4. Conclusion

In summary, N-CQDs modified Bi<sub>4</sub>O<sub>5</sub>I<sub>2</sub> hollow nanotube photocatalysts have been synthesized for the first time. As-prepared N-CQDs/Bi<sub>4</sub>O<sub>5</sub>I<sub>2</sub> composites exhibited improved photocatalytic degradation performance of different organic pollutants (BPA, ENR and RhB) with the high cycle stability and broad spectrum photocatalytic performance. After the N-CQDs modified on the surface of Bi<sub>4</sub>O<sub>5</sub>I<sub>2</sub> nanotubes, abundant •O<sub>2</sub><sup>−</sup> was generated for the fascinating electron transfer ability of N-CQDs and further took part in the reaction to produce •OH. These findings provide some deep insight into structure-activity relationship among other N-CQDs modified 1D nanomaterials and manipulation the generation of active species.

#### Acknowledgements

This work was financially supported by the National Natural Science Foundation of China (Nos. 21471069, 21476098 and 21576123), Jiangsu University Scientific Research Funding (No. 11JDG0146), and Doctoral Innovation Fund of Jiangsu Province (KYCX17\_1791).

#### Appendix A. Supplementary data

Supplementary material related to this article can be found, in the online version, at doi:<https://doi.org/10.1016/j.apcatb.2018.06.014>.

## References

- [1] S. Kment, F. Riboni, S. Pausova, L. Wang, L.Y. Wang, H. Han, Z. Hubicka, J. Krysa, P. Schmuki, R. Zboril, *Chem. Soc. Rev.* 46 (2017) 3716–3769.
- [2] G.G. Zhang, Z.A. Lan, X.C. Wang, *Angew. Chem. Int. Ed.* 55 (2016) 15712–15727.
- [3] J. Li, H. Li, G.M. Zhan, L.Z. Zhang, *Acc. Chem. Res.* 50 (2017) 112–121.
- [4] S.M. Sun, X.M. Li, W.Z. Wang, L. Zhang, X. Sun, *Appl. Catal. B* 200 (2017) 323–329.
- [5] X.X. Chang, T. Wang, J.L. Gong, *Energy Environ. Sci.* 9 (2016) 2177–2196.
- [6] S. Gao, B.C. Gu, X.C. Jiao, Y.F. Sun, X.L. Zu, F. Yang, W.G. Zhu, C.M. Wang, Z.M. Feng, B.J. Ye, Y. Xie, *J. Am. Chem. Soc.* 139 (2017) 3438–3445.
- [7] J.X. Low, J.G. Yu, M. Jaroniec, S. Wageh, A.A. Al-Ghamdi, *Adv. Mater.* 29 (2017) 1601694.
- [8] S.L. Wang, S.H. Lin, D.Q. Zhang, G.S. Li, M.K.H. Leung, *Appl. Catal. B* 215 (2017) 85–92.
- [9] J. Tian, Y.H. Leng, Z.H. Zhao, Y. Xia, Y.H. Sang, P. Hao, J. Zhan, M.C. Li, H. Liu, *Nano Energy* 11 (2015) 419–427.
- [10] X.F. Ning, J. Li, B.J. Yang, W.L. Zhen, Z. Li, B. Tian, G.X. Lu, *Appl. Catal. B* 212 (2017) 129–139.
- [11] C. Han, Z. Chen, N. Zhang, J.C. Colmenares, Y.J. Xu, *Adv. Funct. Mater.* 25 (2015) 221–229.
- [12] M.X. Ji, J. Di, Y.P. Ge, J.X. Xia, H.M. Li, *Appl. Surf. Sci.* 413 (2017) 372–380.
- [13] M.L. Li, L.X. Zhang, X.Q. Fan, Y.J. Zhou, M.Y. Wu, J.L. Shi, *J. Mater. Chem. A* 3 (2015) 5189–5196.
- [14] H.W. Huang, X.W. Li, J.J. Wang, F. Dong, P.K. Chu, T.R. Zhang, Y.H. Zhang, *ACS Catal.* 5 (2015) 4094–4103.
- [15] H. Wang, Wd. Zhang, X.W. Li, J.Y. Li, W.L. Cen, Q.Y. Li, F. Dong, *Appl. Catal. B* 225 (2018) 218–277.
- [16] J.J. Yang, D.M. Chen, Y. Zhu, Y.M. Zhang, Y.F. Zhu, *Appl. Catal. B* 205 (2017) 228–237.
- [17] W.J. He, Y.J. Sun, G.M. Jiang, H.W. Huang, X.M. Zhang, F. Dong, *Appl. Catal. B* 232 (2018) 340–347.
- [18] J.Y. Li, X.A. Dong, Y.J. Sun, W.L. Cen, F. Dong, *Appl. Catal. B* 226 (2018) 269–277.
- [19] J. Li, G.M. Zhan, Y. Yu, L.Z. Zhang, *Nat. Commun.* 7 (2016) 11480.
- [20] J. Di, J.X. Xia, M.X. Ji, L. Xu, S. Yin, Z.G. Chen, H.M. Li, *J. Mater. Chem. A* 4 (2016) 5051–5061.
- [21] A. Henriqueza, H.D. Mansilla, A.M.M.L. Cruz, J. Freer, D. Contreras, *Appl. Catal. B* 206 (2017) 252–262.
- [22] H. Li, F. Qin, Z.P. Yang, X.M. Cui, J.F. Wang, L.Z. Zhang, *J. Am. Chem. Soc.* 139 (2017) 3513–3521.
- [23] J. Di, C. Chen, S.Z. Yang, M.X. Ji, C. Yan, K.Z. Gu, J.X. Xia, H.M. Li, S.Z. Li, Z. Liu, *J. Mater. Chem. A* 5 (2017) 14144–14151.
- [24] H. Li, J. Li, Z.H. Ai, F.L. Jia, L.Z. Zhang, *Angew. Chem. Int. Ed.* 57 (2018) 122–138.
- [25] X.J. Wen, C.G. Niu, L. Zhang, G.M. Zeng, *ACS Sustain. Chem. Eng.* 5 (2017) 5134–5147.
- [26] M.J. Islam, H.K. Kim, D.A. Reddy, Y.J. Kim, R. Ma, H.Y. Baek, J.H. Kim, T.K. Kim, *Dalton Trans.* 46 (2017) 6013–6023.
- [27] R.F. Dong, Y. Hu, Y.F. Wu, W. Gao, B.Y. Ren, Q.L. Wang, Y.P. Cai, *J. Am. Chem. Soc.* 139 (2017) 1722–1725.
- [28] H.W. Huang, K. Xiao, Y. He, T.R. Zhang, F. Dong, X. Du, Y.H. Zhang, *Appl. Catal. B* 199 (2016) 75–86.
- [29] H.W. Huang, X. Han, X.W. Li, S.C. Wang, P.K. Chu, Y.H. Zhang, *ACS Appl. Mater. Interfaces* 7 (2015) 482–492.
- [30] H.W. Huang, Y. He, X. Du, P.K. Chu, Y.H. Zhang, *ACS Sustain. Chem. Eng.* 3 (2015) 3262–3273.
- [31] J.X. Xia, M.X. Ji, J. Di, B. Wang, S. Yin, Q. Zhang, M.Q. He, H.M. Li, *Appl. Catal. B* 191 (2016) 235–245.
- [32] C.Y. Wang, X. Zhang, H.B. Qiu, G.X. Huang, H.Q. Yu, *Appl. Catal. B* 205 (2017) 615–623.
- [33] Y. Bai, T. Chen, P.Q. Wang, L. Wang, L.Q. Ye, *Chem. Eng. J.* 304 (2016) 454–460.
- [34] Y. Bai, L.Q. Ye, L. Wang, X. Shi, P.Q. Wang, W. Bai, P.K. Wong, *Appl. Catal. B* 194 (2016) 98–104.
- [35] S.Y. Wang, X. Hai, X. Ding, K. Chang, Y.G. Xiang, X.G. Meng, Z.X. Yang, H. Chen, J.H. Ye, *Adv. Mater.* 29 (2017) 1701774.
- [36] J. Li, L.J. Cai, J. Shang, Y. Yu, L.Z. Zhang, *Adv. Mater.* 28 (2016) 4059–4064.
- [37] Y. Bai, L.Q. Ye, T. Chen, L. Wang, X. Shi, X. Zhang, D. Chen, *ACS Appl. Mater. Interfaces* 8 (2016) 27661–27668.
- [38] H.W. Huang, K. Xiao, T.R. Zhang, F. Dong, Y.H. Zhang, *Appl. Catal. B* 203 (2017) 879–888.
- [39] G.J. Wu, Y. Zhao, Y.W. Li, F.N. Zhang, J.Z. Zhao, *CrystEngComm* 19 (2017) 2113–2125.
- [40] Q.C. Liu, D.K. Ma, Y.Y. Hu, Y.W. Zeng, S.M. Huang, *ACS Appl. Mater. Interfaces* 5 (2013) 11927–11934.
- [41] X.L. Jin, C.D. Lv, X. Zhou, C.M. Zhang, Q.Q. Meng, Y. Liu, G. Chen, *Appl. Catal. B* 226 (2018) 53–60.
- [42] N. Wei, H.Z. Cui, X.Z. Wang, X. Xie, M.L. Wang, L.Q. Zhang, J. Tian, *J. Colloid Interface Sci.* 498 (2017) 263–270.
- [43] Z. Li, H.J. Yu, T. Bian, Y.F. Zhao, C. Zhou, L. Shang, Y.H. Liu, L.Z. Wu, C.H. Tung, T.R. Zhang, *J. Mater. Chem. C* 3 (2015) 1922–1928.
- [44] S.W. Cao, J.G. Yu, *J. Photochem. Photobiol. C* 27 (2016) 72–99.
- [45] M.X. Ji, J.X. Xia, J. Di, B. Wang, S. Yin, L. Xu, J.Z. Zhao, H.M. Li, *J. Colloid Interface Sci.* 478 (2016) 324–333.
- [46] J. Di, J.X. Xia, M.X. Ji, H.P. Li, H. Xu, H.M. Li, R. Chen, *Nanoscale* 7 (2015) 11433–11443.
- [47] J.X. Xia, M.X. Ji, J. Di, B. Wang, S. Yin, M.Q. He, Q. Zhang, H.M. Li, *J. Alloys Compd.* 695 (2017) 922–930.
- [48] X. Xiao, S.H. Tu, M.L. Lu, H. Zhong, C.X. Zheng, X.X. Zuo, J.M. Nan, *Appl. Catal. B* 198 (2016) 124–132.
- [49] X. Xiao, C.L. Xing, G.P. He, X.X. Zuo, J.M. Nan, L.S. Wang, *Appl. Catal. B* 148–149 (2014) 154–163.
- [50] S.S. Fang, M. Lu, M. Zhou, Z.Y. Li, S. Xu, Y.Y. Peng, Q.C. Li, D.Y. Lu, *Acta Phys. Pol. A* 131 (2017) 263–270.
- [51] F. Tian, H.P. Zhao, Z. Dai, G. Cheng, R. Chen, *Ind. Eng. Chem. Res.* 55 (2016) 4969–4978.
- [52] W.L. Zhang, Y.L. Cao, P.Y. Tian, F. Guo, Y. Tian, W. Zheng, X.Q. Ji, J.Q. Liu, *ACS Appl. Mater. Interfaces* 8 (2016) 32440–32449.
- [53] J.X. Xia, J. Di, H.T. Li, H. Xu, H.M. Li, S.J. Guo, *Appl. Catal. B* 181 (2016) 260–269.
- [54] H. Wang, D.Y. Yong, S.C. Chen, S.L. Jiang, X.D. Zhang, W. Shao, Q. Zhang, W.S. Yan, B.C. Pan, Y. Xie, *J. Am. Chem. Soc.* 140 (2018) 1760–1766.
- [55] H.W. Huang, S.C. Tu, C. Zeng, T.R. Zhang, A.H. Reshak, Y.H. Zhang, *Angew. Chem. Int. Ed.* 56 (2017) 11860–11864.
- [56] M.X. Ji, J.X. Xia, J. Di, Y.L. Liu, R. Chen, Z.G. Chen, S. Yin, H.M. Li, *Chem. Eng. J.* 331 (2018) 355–363.
- [57] H.W. Huang, Y. He, X.W. Li, M. Li, C. Zeng, F. Dong, X. Du, T.R. Zhang, Y.H. Zhang, *J. Mater. Chem. A* 3 (2015) 24547–24556.
- [58] H.W. Huang, R.R. Cao, S.X. Yu, K. Xu, W.C. Hao, Y.G. Wang, F. Dong, T.R. Zhang, Y.H. Zhang, *Appl. Catal. B* 219 (2016) 526–537.
- [59] G. Liu, L.Z. Wang, C.H. Sun, X.X. Yan, X.W. Wang, Z.G. Chen, S.C. Smith, H.M. Cheng, G.Q. Lu, *Chem. Mater.* 21 (2009) 1266–1274.